Fasudil prevents neomycin-induced hair cell damage by inhibiting autophagy through the miR-489/NDP52 signaling pathway in HEI-OC1 cells

WEI LI[1*], YANQIU ZHANG[2*], JIFENG XU[3], JINCAN CHEN[3] and XIA GAO[4,5]

[1]Department of Otolaryngology Head and Neck Surgery, The Affiliated Hospital of Xuzhou Medical University, Xuzhou, Jiangsu 221006; [2]Department of Otolaryngology Head and Neck Surgery, Xuzhou Cancer Hospital, Xuzhou, Jiangsu 221005; [3]Department of Otolaryngology Head and Neck Surgery, The First Clinical Medical College of Xuzhou Medical University, Xuzhou, Jiangsu 221004; [4]Research Institute of Otolaryngology; [5]Department of Otolaryngology Head and Neck Surgery, Gulou Hospital Affiliated to Medical College of Nanjing University, Nanjing, Jiangsu 210008, P.R. China

Received November 11, 2020; Accepted August 11, 2021

DOI: 10.3892/etm.2021.10965

Abstract. Hearing loss is a common sensory disorder that is mainly caused by the loss of hair cells (HCs). Drug-induced deafness, for which there is currently no effective treatment, is mainly caused by the inappropriate use of aminoglycoside antibiotics. Fasudil (Fas), a novel isoquinoline sulfonamide derivative, has exhibited antioxidant abilities in a number of previous studies. The aim of the present study was to investigate the potential effects of Fas against neomycin (Neo)-induced hair cell damage and elucidate the underlying mechanism. Flow cytometry and western blot analysis were used to detect the effects of Fas on cell apoptosis and to determine the expression levels of autophagy-related proteins, LC3B and Beclin 1, induced by Neo. Mitochondrial membrane potential and reactive oxygen species (ROS) levels were detected using fluorescent probes. The effect of Fas on Neo-induced hair cell injury marker, GFP-LC3B, was also examined using the immunofluorescence technique. Fas was found to inhibit Neo-induced mitochondrial autophagy and mitochondrial membrane potential decline, in addition to reducing ROS levels and cell apoptosis caused by Neo treatment. However, Fas failed to inhibit the Neo-induced these above changes in cells with NDP52 overexpression. The putative binding sites of microRNA (miR)-489 on the 3'-untranslated region of nuclear dot protein 52 (NDP52) were predicted using the TargetScan 7.0 online tool, and this association was further verified using a dual-luciferase reporter assay. Moreover, the expression of miR-489 negatively regulated the expression of NDP52. Fas and miR-489 mimic inhibited the Neo-induced mitochondrial autophagy and mitochondrial membrane potential decline, in addition to reducing ROS levels and cell apoptosis. Knockdown of miR-489 expression using a miR-489 inhibitor blocked the inhibitory effects of Fas on the mitochondrial membrane potential, cell apoptosis and ROS production. Therefore, Fas may upregulate the expression of miR-489 to negatively regulate the expression of NDP52 at the post-transcriptional level, which in turn inhibits the activation of mitophagy and cell injury induced by Neo. Thus, Fas may act as a novel therapeutic option in the clinical treatment of hearing loss in the future.

Correspondence to: Dr Xia Gao, Department of Otolaryngology Head and Neck Surgery, Gulou Hospital Affiliated to Medical College of Nanjing University, 321 Zhongshan Road, Gulou, Nanjing, Jiangsu 210008, P.R. China
E-mail: xiagao2020@163.com

*Contributed equally

Key words: fasudil, aminoglycosides, hair cells, apoptosis, microRNA

Introduction

Sensorineural hearing loss is a type of auditory impairment that is caused by congenital genetics, such as SCN11A gene deletion impairing the ribbon synapses and auditory nerves, or acquired factors, such as ototoxic drugs (1-3). As a result, the hearing system abnormally perceive and process sound (4). The main pathological manifestation of this condition is damage to the inner ear cochlear hair cells (5). In total, >30% patients who are deaf are afflicted with drug-induced deafness, which is mainly caused by the improper use of aminoglycoside antibiotics, such as neomycin (Neo) and streptomycin, with ~5% of patients exhibiting significant hearing loss using such antibiotics (6-8). In particular, Neo has a high incidence of hearing loss worldwide, compared with other aminoglycoside antibiotics (3). Since aminoglycoside antibiotics are widely used in developed countries (9), protecting hair cells and reducing the damage caused by aminoglycoside antibiotics currently represents a challenge.

Hair cells are receptors in the ear that produce auditory impulses (2), which cannot regenerate if destroyed (10). Ear damage can lead to irreversible injury of cochlear hair cells and auditory neurons, leading to permanent sensorineural

deafness (11). Common environmental factors that cause sensorineural deafness include perinatal infection, excessive noise, aging and ototoxic drugs (3,12). Specifically, noise, aging and ototoxic drugs can induce hair cell death through oxidative stress or activation of apoptotic pathways (13,14). It has been previously demonstrated that the mechanism underlying ototoxicity of aminoglycoside antibiotics is mainly through damage and apoptosis of hair cells, resulting in permanent hearing loss and vestibular dysfunction (15). After the drugs enter the cochlea, the increase in reactive oxygen species (ROS) and calcium ions in sensory cells and neurons of the inner ear disrupts physiological mitochondrial protein synthesis and reduces the mitochondrial membrane potential, in turn promoting the release of cytochrome c into the cytosol (16). Therefore, local or systemic application of ROS scavengers may protect the cochlea from aminoglycoside antibiotics (17). Calcium-activated protease, such as Calpain, also served an important role in the destruction of hair cells caused by aminoglycoside antibiotics (18). Therefore, inhibiting the activity of calcium-activated proteases may also effectively protect cochlear hair cells from drug-induced damage (15).

Fasudil (Fas) is a novel isoquinoline sulfonamide derivative that was originally developed as an effective Rho kinase (ROCK) inhibitor and calcium ion antagonist (19). Fas is the only ROCK inhibitor currently approved for a number of brain disorders in humans, including ischemia-reperfusion injury, brain edema, and cerebral microthrombosis (20). It has few side effects and was approved by Japan in 1995 for the clinical treatment of subarachnoid hemorrhage caused by cerebral vasospasm (21). Vasoconstriction and Ca^{2+} sensitization induced by ROCK can both be alleviated and eliminated by Fas, where the pharmacological effects of this ROCK inhibitor are proposed to be mediated by the downregulation of ROCK expression/activity under pathobiological conditions (22,23). Studies have previously shown that ROS can cause the activation of the RhoA/ROCK signaling pathway (24-27). Therefore, using Fas to inhibit RhoA/ROCK signaling reduced oxidative stress in Neo-induced hair cell damage (7,28), suggesting that Fas may exert a protective effect against aminoglycoside-induced damage of the inner ear hair cells. Zhang *et al* (7) previously found that Fas pre-treatment can significantly inhibit the Rho signaling pathway after exposure to Neo in hair cells, further reducing the accumulation of ROS and cell apoptosis induced by Neo.

MicroRNAs (miRNAs/miRs) are a class of non-coding single-stranded RNA molecules with a length of 22 nucleotides (29). They are involved in the regulation of gene expression on a post-transcriptional level in plants and animals, and can therefore regulate various physiological and pathological processes, including antibacterial resistance, cell proliferation, autophagy and apoptosis (30-32). miRNAs recognize and bind to complementary target sequences in the 3'-untranslated region (UTR) region of target mRNA sequences, leading to mRNA degradation and inhibition of target gene translation (33). miR-489 has been shown to inhibit a number of different cancers, including osteosarcoma, gastric, lung, ovarian, liver and bladder cancer (34-36). Soni *et al* (37) previously reported that miR-489 could affect the expression of several genes, such as LAPTM4B involved in autophagy in breast cancer cells. Liao *et al* (38) pointed out miR-489 specifically by inhibiting autophagy by targeting Unc-51 like autophagy activating kinase and lysosomal protein transmembrane 4β in ovarian cancer cells.

Therefore, the present study was undertaken to investigate the effects of Fas on the cochlear hair cell line HEI-OC1 following induction by Neo. In addition, the present study determined whether its effects were mediated by regulating the expression of miR-489 and the autophagy-related nuclear dot protein 52 (NDP52) en route to regulating Neo-induced autophagy and hair cell injury.

Materials and methods

Cell culture. The HEI-OC1 mouse inner ear hair cell line, originated from House Ear Institute (https://houseinstitute.com/), was purchased from Biofeng (cat. no. CVCL_D899; http://www.biofeng.com/xibao/xibaozhu/HEI-OC1.html) and cultured in high-glucose DMEM supplemented with 10% FBS. All cell culture media and reagents were purchased from Gibco; Thermo Fisher Scientific, Inc. All cells were incubated in 5% CO_2 at 37˚C. When the cell confluence reached 80%, subculture was conducted.

Flow cytometry. Flow cytometry was performed with a PI/Annexin V Cell Apoptosis Detection kit (Sigma-Aldrich; Merck KGaA) according to the manufacturer's protocols. Briefly, the HEI-OC1 cells were inoculated into 6-well plates and divided into Control, Neo, Neo + Fas/Low, Neo + Fas/Mid and Neo + Fas/High groups. When the cells grew to ~70% confluence, 5 mM Neo was added. Fas was administered at 5, 10 and 20 μM doses for low, medium and high groups, respectively. Fas was added to the treatment groups for 1 h prior to Neo induction. After 24 h of treatment at room temperature, the cells at a density of $1x10^5$ cell/well were collected and washed with binding buffer prior to staining with Annexin V-FITC and PI (5 μl). The percentage of both early and late apoptotic cells was calculated using flow cytometry (BD FASCanto™ II; BD Biosciences). The apoptosis analysis was performed by FlowJo V10 software (version 10; Emerald Biotech Co., Ltd).

Cell treatment. Cells were cultured at a density of $1x10^5$ cell/well and 5 mM Neo was added to each well. The medium dose of Fas (10 μM) was administered to the treatment groups for 1 h prior to Neo induction, which was used in the following experiments.

Transient transfection assay. Recombinant adenovirus vector plasmid of NDP52 overexpression (Ad5-EGFP-NDP52 OE) and control plasmid (Ad5-EGFP) were synthesized by Beijing SinoGenoMax Research Center Co., Ltd. miR-489 mimic (5'-GUGACAUCACAUAUACGGCAGC-3'), miR-negative control (NC) mimic (5'-UUGUCCGAACGUGUCACGUTT-3'), miR-489 inhibitor (5'- GCTGCCGTATATGTGATGTCAC-3') and miR-NC inhibitor (5'-CAGUACUUUUGUGUAGUACAA-3') were purchased from Guangzhou RiboBio Co., Ltd.

For adenovirus infection, HEI-OC1 cells were seeded in 6-well plates at a density of $1x10^6$ cell/well and infected with 100 MOI adenovirus for 2 days. When ~80% confluence was

reached, HEI-OC1 cells were transfected with 30 nM plasmid overexpression vectors, miR-489 mimic, miR-489 inhibitor or the negative control using Lipofectamine® 2000 (Thermo Fisher Scientific, Inc.) for 2 days at 37˚C, according to the manufacturer's protocols. Subsequently, cells were treated with 5 mM Neo and/or 10 μM Fas.

Reverse transcription-quantitative PCR (RT-qPCR). Total RNA was isolated from cultured cells by using TRIzol® reagent (Thermo Fisher Scientific, Inc.) and 1 μg total RNA was reverse-transcribed into cDNA by using AMV Reverse Transcriptase XL*1 (5 U/μl; Takara Bio, Inc.) and a RT primer according to the manufacturer's protocols. The temperature protocol was as follows: 16˚C for 30 min, 42˚C for 30 min and 85˚C for 5 min. qPCR was performed using a VetMAX™-Plus One-Step RT-PCR kit (Applied Biosystems; Thermo Fisher Scientific, Inc.) by following the manufacturer's protocols with U6 as the internal control. GAPDH was used as reference control for NDP52. The sequences of the primers were as follows: miR-9 forward, 5'-AGCTTGCTGCACCTTAGTCT-3' and reverse, 5'-TGTGTGCGGCTAGAACATCC-3'; miR-34a forward, 5'-GCGCGCAATCAGCAAGTATAC-3' and reverse, 5'-AGTGCAGGGTCCGAGGTATT-3'; miR-489 forward, 5'-ACACTCCAGCTGGGGTGACATCACATA-3' and reverse, 5'-TGGTGTCGTGGAGTCG-3'; miR-23a forward, 5'-GGGGGTTCCTGGGGATG-3' and reverse, 5'-AGTGCAG GGTCCGAGGTATT-3'; miR-494 forward, 5'-CGCGTG AAACATACACGGGA-3' and reverse, 5'-AGTGCAGGG TCCGAGGTATT-3'; miR-93 forward, 5'-CAAAGUGCU GUUCGUGCAGGUAG-3' and 5'-AGTGCAGGGTCCGAG GTATT-3'; miR-214 forward, 5'-GCGACAGCAGGCACA GACA-3' and reverse, 5'-AGTGCAGGGTCCGAGGTATT-3'; NDP52 forward, 5'-GACAACCCGTGAGTATTACACC-3' and reverse, 5'-TGGAAAGGAATACTTGCTCCC-3'; U6 forward, 5'-GCTTCGGCAGCACATATACTAAAAT-3' and reverse, 5'-CGCTTCACGAATTTGCGTGTCAT-3'; and GAPDH forward, 5'-AGCAGTCCCGTACACTGGCAAAC-3' and reverse, 5'-TCTGTGGTGATGTAAATGTCCTCT-3'. The reactions were performed in a 96-well plate at 95˚C for 10 min, followed by 40 cycles at 95˚C for 10 sec and 60˚C for 1 min. The relative gene expression levels were normalized to the level of the endogenous control GAPDH, and were calculated using the $2^{-\Delta\Delta CT}$ method (39).

Western blot analysis. Total protein was extracted from cells with RIPA lysis buffer (Beyotime Institute of Biotechnology). After measuring the protein concentrations using the Bradford assay, 40 μg protein was loaded, separated by using 10% SDS-PAGE and then transferred onto PVDF membranes (Merck KGaA). Next, the membranes were incubated with 0.5% bovine serum albumin (Gibco; Thermo Fisher Scientific, Inc.) for 1 h at room temperature, followed by washing in PBS. The membranes were then incubated with primary antibodies at 4˚C overnight, followed by washing and incubation in HRP-conjugated secondary antibodies (1:2,000; cat. no. A0208; Beyotime Institute of Biotechnology) at room temperature for 1-2 h. The primary antibodies used were anti-NDP52 (1:1,000, cat. no. ab68588; Abcam), anti-LC3B (1:1,000, cat. no. ab51520; Abcam) and anti-Beclin 1 (1:1,000, cat. no. ab210498; Abcam). GAPDH (1:2,000, cat. no. ab9485; Abcam) served as a loading control. Finally, the bands were evaluated using scanning densitometry (ImageQuant™ LAS4000; Cytiva) and analyzed using ImageJ software (version V1.0.8; National Institutes of Health) following Pierce™ ECL Plus Western Blotting Substrate treatment (Thermo Fisher Scientific, Inc.).

Dual-luciferase reporter assay. HEI-OC1 cells were cultured in six-well plates at a density of $1x10^6$ cell/well. TargetScan (http://www.targetscan.org/vert_70/), miRWalk (http://mirwalk.umm.uni-heidelberg.de/), miRNet (https://www.mirnet.ca/miRNet/home.xhtml), miRDB (http://mirdb.org/), microT-CDS (http://diana.imis.athena-innovation.gr/DianaTools/index.php?r=microT_CDS/index), miRSystem (https://tools4mirs.org/software/target_functional_analysis/mirsystem/) and miRNA MAP (http://mirnamap.mbc.nctu.edu.tw./) were used to predict microRNAs that may target the NDP52 mRNA 3'-UTR.The putative binding sites of miR-489 on the NDP52 3'-UTR were predicted using the TargetScan 7.0 (http://www.targetscan.org/vert_70/) online tool. The NDP52 3'-UTR sequences were chemically synthesized by Guangzhou RiboBio Co., Ltd. and introduced into the luciferase reporter vector (pGL3-Basic) to construct wild-type (WT) luciferase reporter plasmids (NDP52 WT), and the seed regions of miR-489 in the 3'-UTR of NDP52 were mutated to construct mutant (MUT) luciferase reporter plasmids (NDP52 MUT). HEI-OC1 cells were co-transfected with 0.5 μg/µl luciferase reporter plasmids (NDP52 WT or NDP52 MUT in the pGL3-Basic vector; Guangzhou RiboBio Co., Ltd.), miR-489 mimics or inhibitors, and their negative control using Lipofectamine® 2000 (Thermo Fisher Scientific, Inc.). After 48 h, the cells were collected and measured using the Dual-Luciferase Reporter Assay (Promega Corporation) according to the manufacturer's protocols. The dual-luciferase activity of the target gene was normalized to *Renilla* luciferase activity.

MitoTracker mitochondrial staining. MitoTracker (Thermo Fisher Scientific, Inc.) was added to serum-free DMEM (Gibco; Thermo Fisher Scientific, Inc.) and diluted to a concentration of 200 nM, before the cell culture medium was replaced with this serum-free medium containing 200 nM MitoTracker, followed by incubation at 37˚C for 25 min. After incubation, the cells were washed with serum-free medium and staining was observed under a fluorescence microscope (magnification, x200; Zeiss 710; Carl Zeiss AG).

Mitochondrial membrane potential detection. The mitochondrial membrane potential was detected using JC-1 fluorescence mitochondrial imaging (40). JC-1 (200X; cat. no. C2006; Beyotime Institute of Biotechnology) was diluted by adding ultra-pure water (ddH_2O) following the addition of JC-1 buffer (5X) to prepare JC-1 staining buffer (1X). The cells at a density of $1x10^5$ cell/well were incubated with JC-1 staining solution (1X) at 37˚C for 20 min. After incubation, the supernatant was removed and cells were washed with JC-1 staining buffer (1X) for two times. DAPI (100 ng/ml; Beijing Solarbio Science & Technology Co., Ltd.) was used for counterstaining of the cell nuclei at 37˚C

for 10 min and the cells were observed under a fluorescence microscope (magnification, x200; ZEISS 710; Carl Zeiss AG). When detecting JC-1 monomer (green), excitation was set at 490 nm and the emission was set at 530 nm. For the detection of JC-1 aggregation (red), excitation light was set at 525 nm and the emission was set at 590 nm. The ratio of red to green fluorescence represented the mitochondrial membrane potential.

Mitochondrial autophagy detection. Mitochondrial autophagy was detected by transfection of the green fluorescent protein GFP-LC3B plasmid synthesized by Nanjing GenScript Biotechnology Co., Ltd. and combined with MitoTracker Red (Beyotime Institute of Biotechnology) fluorescence staining. HEI-OC1 cells at a density of $1x10^5$ cell/well were cultured in 24-well plates. The cells were divided into the following three groups: Control group, Neo group and Neo + Fas group. The GFP-LC3B plasmid (500 ng), P3000™ reagent (1 μl; Thermo Fisher Scientific, Inc.; used to enhance the cell transfection efficiency of Lipofectamine 3000) and Lipofectamine 3000 (1 μl; Thermo Fisher Scientific, Inc.) were added into the fresh culture medium (50 μl) for 20 min at room temperature and the aforementioned medium was added into each well, and cultured for a further 8 h, according to the manufacturer's protocol. MitoTracker Red working solution (PBS diluted) with a concentration of 25 nM was prepared and put into the cell culture incubator for preheating. After rinsing the cells with PBS three times, the MitoTracker Red working solution was added to the cells at 500 μl/well (final concentration, 12.5 μM) and incubated at 37˚C for 20 min. After the incubation, the cells were washed three times with pre-cooled PBS, and DAPI (100 ng/ml; Beijing Solarbio Science & Technology Co., Ltd.) was used for counterstaining of the cell nuclei at 37˚C for 10 min. Then, cells were observed under a fluorescence microscope at x200 magnification (ZEISS 710; Carl Zeiss AG). Green light represents the position of GFP-LCB and red light represents the position of mitochondria. The superposition of green fluorescence and red fluorescence is regarded as autophagy in mitochondria.

Fluorescence detection of intracellular ROS levels. The intracellular ROS levels were examined using 2,7-dichlorfluoresceindiacetate staining (DCFH-DA; Beyotime Institute of Biotechnology) according to the manufacturer's protocols. Briefly, the number of cells in each group after drug treatment was adjusted to $1x10^6$-$2x10^7$. DCFH-DA was diluted in serum-free DMEM at 1:1,000 to a final concentration of 10 μM. The cells were collected and suspended in the DCFH-DA-containing serum-free medium to a cell concentration of $1x10^6$-$2x10^7$/ml. The cells were incubated at 37˚C for 20 min. The cells were then washed three times with serum-free DMEM to fully remove DCFH-DA that did not enter the cells. Flow cytometry (BD Biosciences) was used for detection of the fluorescence intensity of intracellular ROS using 488 nm excitation wavelength and 525 nm emission wavelength. The fluorescence analysis was performed by FlowJo V10 software (version 10; Emerald Biotech Co., Ltd)

Statistical analysis. All values are presented as the mean ± SEM from three independent experiments. Statistical analysis was performed by using one-way ANOVA followed by Bonferroni's test for selected pairs using the GraphPad Prism 5 statistical software (GraphPad Software, Inc.). $P<0.05$ was considered to indicate statistically significant difference.

Results

Fas inhibits Neo-induced ototoxicity at the cellular level. Neo exhibits strong ototoxicity and can induce hair cell death (41). To investigate the effect of Fas on ototoxicity induced by Neo at the cellular level, flow cytometry was used to analyze Fas- and Neo-treated HEI-OC1 hair cells. The results demonstrated that Neo significantly increased HEI-OC1 cell apoptosis, whilst Fas significantly inhibited Neo-induced apoptosis of HEI-OC1 cells in a dose-dependent manner (Fig. 1A and B). Since Fas at 5, 10 and 20 μM all exerted satisfactory effects, the medium dose of Fas (10 μM) was selected for subsequent experiments.

Previous studies have shown that Neo induces autophagy in hair cells, which plays an important role in their survival (42,43). In addition, Fas has been reported to inhibit angiotensin-II-induced autophagy of podocytes as a ROCK inhibitor (44). Therefore, the effects of Neo and Fas on autophagy in hair cells of the inner ear were examined. Western blotting was used to detect the protein expression of the autophagy-related markers LC3B and Beclin 1. Neo significantly increased the LC3B-II/LC3B-I ratio and Beclin 1 expression in HEI-OC1 cells, suggesting that Neo induced activation of inner ear hair cell autophagy (Fig. 1C and D). Fas markedly reversed Neo-induced increases of LC3B-II/LC3B-I ratio and Beclin 1 expression (Fig. 1C and D), suggesting that Fas inhibited Neo-induced activation of autophagy in hair cells. Cell autophagy can be divided into non-selective autophagy or the specific autophagy of organelles, including mitochondrial, peroxidase, endoplasmic reticulum and ribosomal autophagy (45-47). Furthermore, it has been previously reported that mitochondrial fragmentation and reductions in the membrane potential are conditions for mitochondrial autophagy (48-50). Therefore, it was explored in the present study whether the effect of Fas on Neo-induced autophagy was selective or non-selective. As displayed in Fig. 1E, following Neo treatment, GFP-LC3B was increased and co-localized with the mitochondria, highlighted by Mito Tracker, compared with the control group. These findings suggested mitochondrial autophagy was activated. However, green fluorescence was reduced in the Neo + Fas group compared with the Neo group, suggesting that Neo-induced mitochondrial autophagy was suppressed by Fas.

Subsequently, JC-1 and the fluorescent probe DCFH-DA were used to detect the effects of Neo and Fas on the mitochondrial membrane potential and the level of ROS in hair cells, respectively. Following treatment with Neo, green fluorescence increased and red fluorescence decreased, suggesting that Neo induced a reduction in the mitochondrial membrane potential of hair cells (Fig. 1F). By contrast, in cells treated with Fas, the effect of Neo on the mitochondrial membrane potential of hair cells was reversed (Fig. 1F). The fluorescent probe DCFH-DA was then used to detect the effects of Neo and Fas on ROS levels in hair cells. As shown in Fig. 1G, Neo increased ROS levels in hair cells, but Fas inhibited the Neo-induced increase in ROS levels (Fig. 1G).

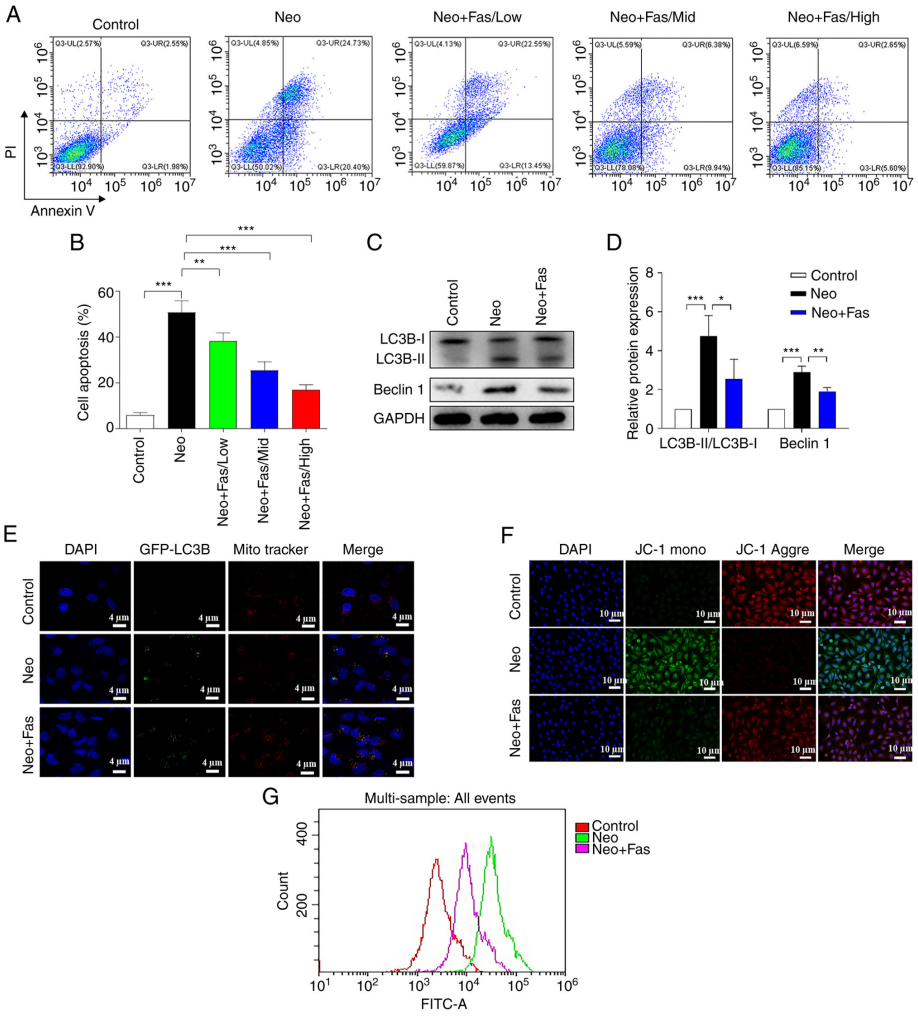

Figure 1. Fas inhibits Neo-induced ototoxicity at the cellular level. HEI-OC1 cells were treated with 5 mM Neo to induce apoptosis. Fas at 10 μM was added 1 h before induction. Testing was performed after 24 h of treatment. (A) Cell apoptosis was detected with flow cytometry after HEI-OC1 cells were treated with Neo and Fas, (B) which was quantified. (C) Western blot analysis of autophagy-associated protein expression s (LC3B and Beclin1). The gray analysis of LC3B and Beclin1 in the control group was classified as 1. (D) Reverse transcription-quantitative PCR was performed to detect the mRNA level of autophagy-associated proteins. (E) Fluorescence images of LC3B-GFP and mitochondria. Red, mitochondria; green, autophagosomes; blue, nucleus. Scale bar, 4 μm. (F) Fluorescence images of HEI-OC1 with JC-1. Red, JC-1 aggregates; green, JC-1 monomers; blue, nucleus. Scale bar, 10 μm. (G) Reactive oxygen species levels were detected with flow cytometry after 2,7-dichlorfluoresceindiacetate staining. Scale bar, 10 μm. n=6 in each group, each independent experiment was repeated three times. Data are expressed as mean ± SEM. *P<0.05, **P<0.01, ***P<0.001. Neo, neomycin; Fas, fasudil; GFP, green fluorescent protein.

Fas inhibits Neo-induced autophagy and cellular injury by reducing NDP52 expression. In the present study, the effect of Neo on the expression of the NDP52 protein in hair cells was investigated. Results of western blotting demonstrated that Neo induced a significant increase in NDP52 protein expression, but Fas significantly inhibited the Neo-induced increase in NDP52 protein levels (Fig. 2A).

To determine whether Fas regulated mitochondrial autophagy by regulating NDP52, NDP52 was overexpressed in hair cells. As shown in Fig. 2B, the results demonstrated that NDP52 expression was significantly increased in cells following transfection with NDP52 overexpression plasmids. The effect of NDP52 overexpression on mitochondrial autophagy was then investigated. As shown in Fig. 2C, overexpression of NDP52 or Neo treatment significantly promoted the activation of autophagy, characterized as the increase of Beclin-1 expression and LC3B II/LC3B I ratio, but Fas significantly inhibited Neo-induced activation of autophagy (Fig. 2C). However, following overexpression of NDP52, the inhibitory effect of Fas on autophagy was weakened or even lost (Fig. 2C).

Mitochondrial colocalization experiments revealed that overexpression of NDP52 and Neo treatment promoted the activation of autophagy. Fas inhibited the Neo-induced activation of autophagy indicated by autophagosomes (green fluorescence) colocalized with mitochondria (red fluorescence). However, following overexpression of NDP52, the inhibitory effect of Fas on autophagy was lost (Fig. 2D), suggesting that Fas may inhibit mitochondrial autophagy by inhibiting NDP52 expression. Measurements of mitochondrial membrane potential revealed that green fluorescence was enhanced after overexpression of NDP52 or Neo treatment, whilst the red fluorescence was decreased, suggesting that Neo induced a decrease in the mitochondrial membrane potential of hair cells (Fig. 2E). Fas reversed the reduction in mitochondrial membrane potential in hair cells induced by Neo (Fig. 2E). However, in cells overexpressing NDP52, Fas failed to inhibit the Neo-induced decrease in the mitochondrial

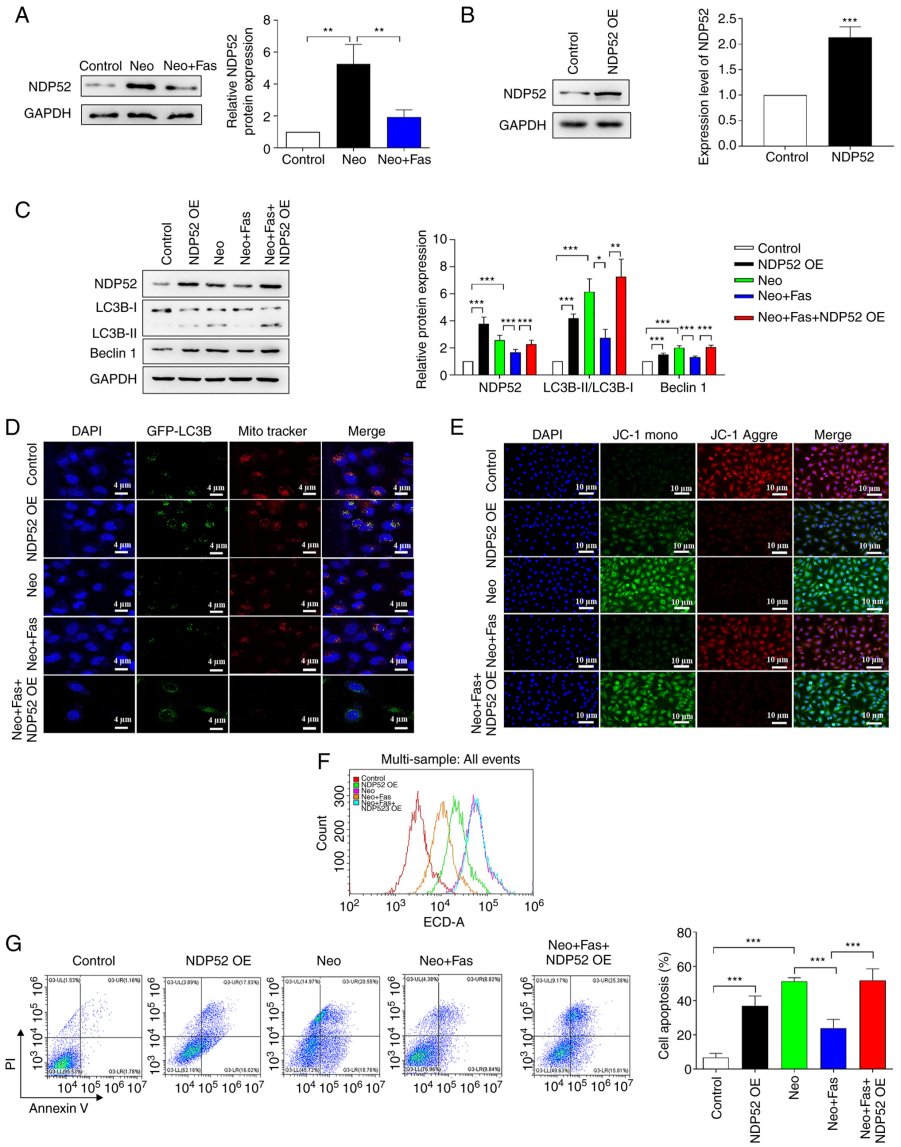

Figure 2. Fas inhibits Neo-induced autophagy and cellular damage by reducing NDP52 expression. (A) Western blot analysis of NDP52 protein expression and grayscale analysis. (B) NDP52 expression was measured in HEI-OC1 cells following transfection with NDP52 plasmids. (C) Western blot analysis of autophagy-associated protein expression and grayscale analysis. The gray analysis of the control group was classified as 1 in western blot analysis. (D) Fluorescence images of GFP-LC3B and mitochondria. Red, mitochondria; green, autophagosome; blue, nucleus. Scale bar, 4 μm. (E) Fluorescence images of HEI-OC1 with JC-1. Red, JC-1 aggregates; green, JC-1 monomer; blue, nucleus. Scale bar, 10 μm. (F) Reactive oxygen species levels were detected with flow cytometry after 2,7-dichlorfluoresceindiacetate staining. (G) Cell apoptosis was detected with flow cytometry after NDP52 plasmid-transfected HEI-OC1 cells were treated with Neo and Fas. n=6 in each group, each independent experiment was repeated three times. Data are expressed as mean ± SEM. *P<0.05, **P<0.01, ***P<0.001. Neo, neomycin; Fas, fasudil; NDP52, nuclear dot protein 52; OE, overexpression; GFP, green fluorescent protein.

membrane potential in hair cells (Fig. 2E). Therefore, these observations suggested that overexpression of NDP52 blocked the inhibitory effects of Fas on the Neo-induced reduction of hair cell mitochondrial membrane potential.

To verify that Fas inhibited Neo-induced hair cell injury by upregulating the expression of NDP52, ROS levels were measured and the results demonstrated that the overexpression of NDP52 or Neo treatment increased the intracellular ROS levels (Fig. 2F). By contrast, ROS levels in cells treated with Fas were markedly lower compared with those induced by Neo (Fig. 2F). However, Fas failed to inhibit the Neo-induced increase in ROS in NDP52-overexpressing cells (Fig. 2F). To verify that the overexpression of NDP52 blocked the inhibitory effect of Fas on Neo-induced hair cell apoptosis, flow cytometry was used to detect apoptosis. Compared with those in the control group, the apoptosis of NDP52-overexpressing and Neo-treated cells was increased significantly (Fig. 2G). Compared with the Neo group, cell apoptosis in the Neo + Fas group was significantly reduced. However, Fas could not inhibit Neo-induced apoptosis in NDP52-overexpressing cells (Fig. 2G).

Fas post-transcriptionally regulates NDP52 expression through miR-489. Thus far, results from the present study suggested that NDP52 is an important factor in mitochondrial autophagy activation, whereas Fas could inhibit mitochondrial autophagy activation by reducing the expression of NDP52. To explore the mechanism through which Fas regulated NDP52 levels, RT-qPCR was used to detect the effect of Neo and Fas on NDP52 mRNA expression. As shown in Fig. 3A, the mRNA

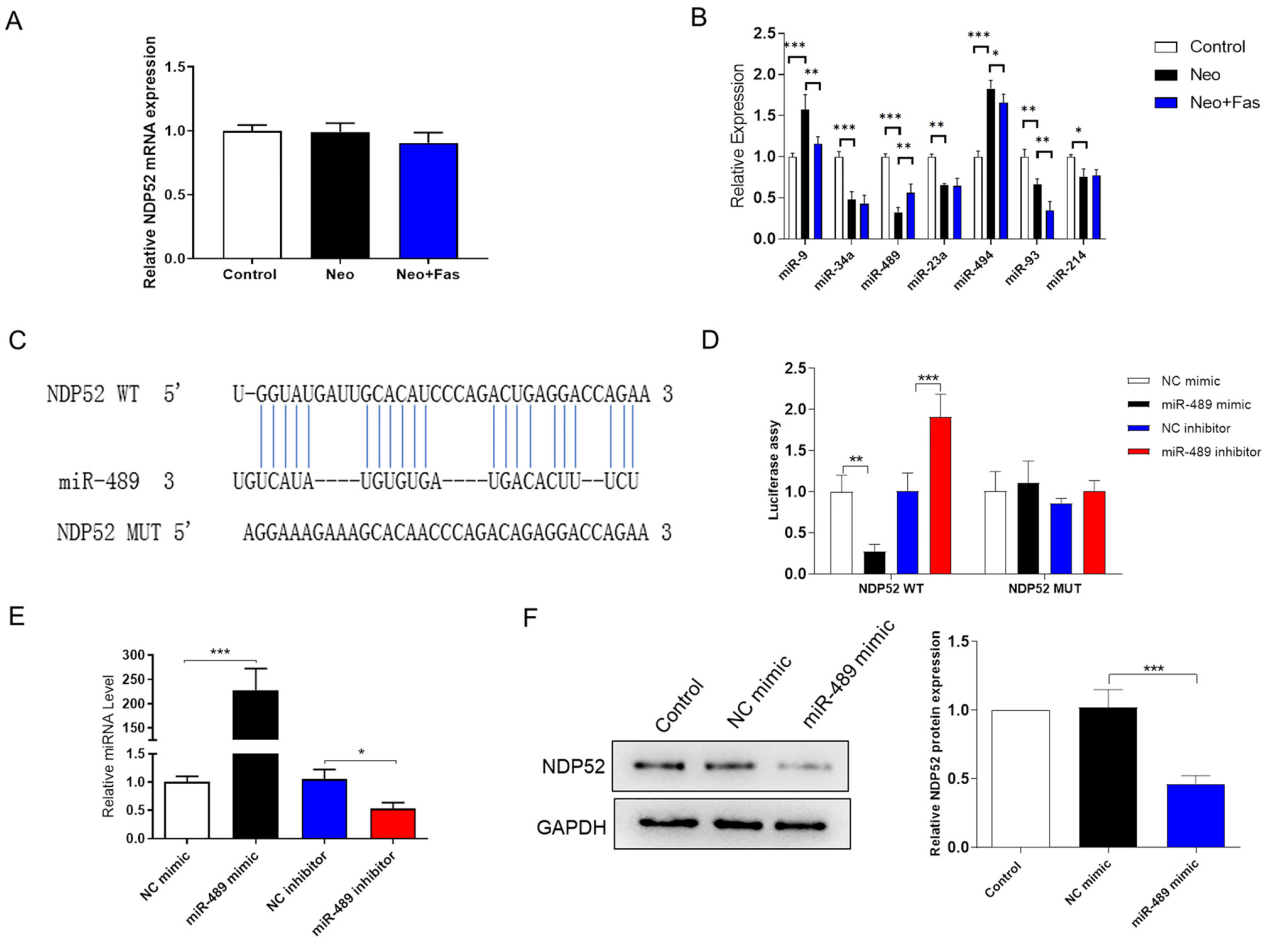

Figure 3. Post-transcriptional regulation of NDP52 by Fas is at least in part mediated by miR-489. (A) Reverse transcription-quantitative PCR was used to detect the effects of Neo and Fas on the mRNA level of NDP52. (B) Expression levels of a panel of miRNAs were detected by reverse transcription-quantitative PCR. (C) Bioinformatics analysis predicted the 3'-UTR binding site of miR-489 on the NDP52 mRNA sequence. (D) Luciferase report assay was used to assess the binding of miR-489 to the 3'-UTR of NDP52 mRNA. (E) Transfection efficiency of the miR-489 mimic and miR-489 inhibitor. (F) Western blotting was used to detect the expression of NDP52 after overexpression of miR-489 in HEI-OC1 cells. The gray analysis of the control group was classified as 1. n=6 in each group, each independent experiment was repeated three times. Data are expressed as mean ± SEM. *P<0.05, **P<0.01, ***P<0.001. NDP52, nuclear dot protein 52; UTR, untranslated region; WT, wild-type; MUT, mutant; NC mimic, negative control mimic; miR, microRNA; Neo, neomycin; Fas, fasudil.

levels of NDP52 both in the Neo and Neo + Fas groups did not change significantly compared with those in control group. As western blotting results (Fig. 2A) demonstrated that Fas could inhibit the Neo-induced increase of NDP52 protein expression, Fas is suggested to regulate the expression of NDP52 at the post-transcriptional level.

Inhibition of target gene expression by miRNAs is a common post-transcriptional regulatory mechanism (51). It is known that the expression level of the miRNA is inversely associated with the expression level of the target protein (31). Therefore, TargetScan, miRWalk, miRNet, miRDB, microT-CDS, miRSystem and miRNA MAP were used to predict microRNAs that may target the NDP52 mRNA 3'-UTR. In total, seven miRNAs (miR-9, miR-34a, miR-489, miR-23a, miR-494, miR-93 and miR-214) were screened out by intersecting with the reported articles associated with deafness and autophagy (31,52-55). RT-qPCR was then used to detect the effect of Fas and Neo on miRNA expression in HEI-OC1 cells. The results shown in Fig. 3B demonstrated that Neo significantly inhibited the expression of miR-489 compared with that in the control group, whilst Fas inhibited the effect of Neo on miR-489 expression. However, the expressions of miR-9, miR-34a, miR-23a, miR-93, and miR-214 were not in accordance with the above trend.

As shown in Fig. 3C, the NDP52 gene was found to contain two putative sites on the 3'-UTR that matched the miR-489 seed region. As shown in Fig. 3D, the miR-489 mimic could inhibit the luciferase activity compared with that transfected with the mimic NC, while the miR-489 inhibitor group enhanced the luciferase activity compared with that in the inhibitor NC group. However, after mutating the binding site of miR-489 in the 3'-UTR region of NDP52, neither the miR-489 mimic nor the miR-489 inhibitor could significantly affect the luciferase activity (Fig. 3D). These results suggested that miR-489 can directly bind to the NDP52 3'-UTR region. The transfection efficiency of the miR-489 mimic and inhibitor was verified by RT-qPCR (Fig. 3E). Western blotting was then used to detect the expression of NDP52 in HEI-OC1 cells after miR-489 overexpression. The results demonstrated that the miR-489 mimic significantly reduced the protein expression of NDP52 compared with that in cells transfected with the mimic NC (Fig. 3F).

Fas inhibits Neo-induced autophagy and cellular damage by increasing miR-489 levels. To explore the role of miR-489

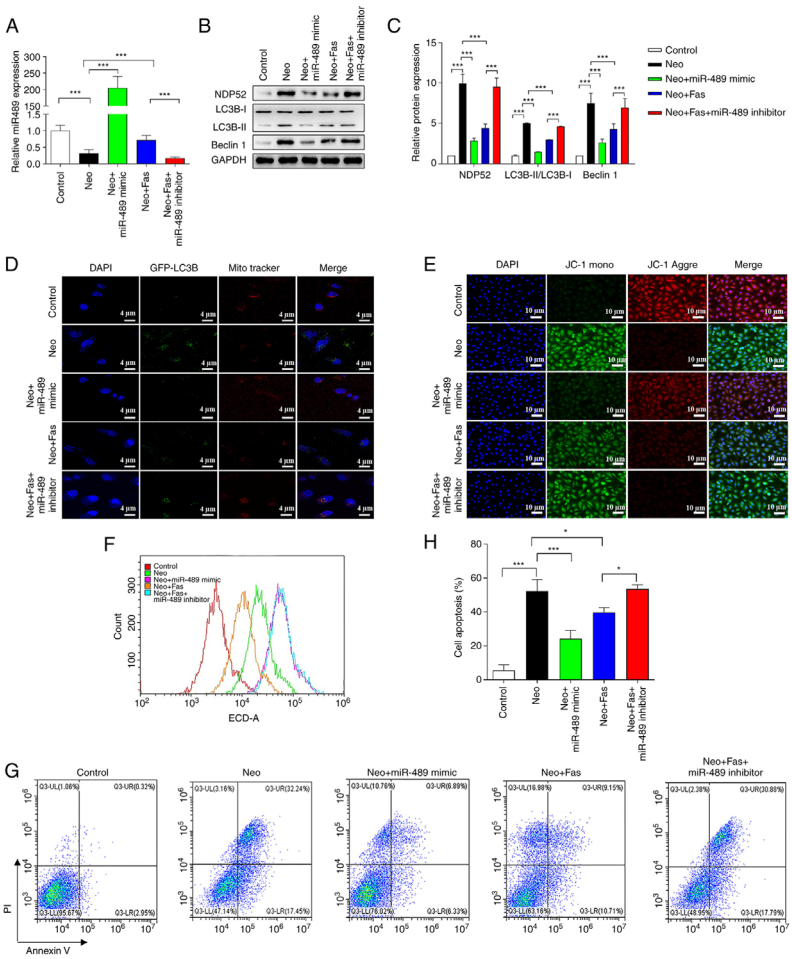

Figure 4. Fas inhibits Neo-induced autophagy and cellular injury by increasing miR-489 levels. (A) miR-489 expression in each treatment group was detected by reverse transcription-quantitative PCR. (B) Western blotting was used to detect the expression of autophagy-related proteins in HEI-OC1 cells after overexpression or knockdown of miR-489. (C) ImageJ software grayscale analysis. The gray analysis of the control group was classified as 1. (D) Fluorescence images of GFP-LC3B and mitochondria. Red, mitochondria; green, autophagosome; blue, nucleus. Scale bar, 4 μm. (E) Fluorescence images of HEI-OC1 cells with JC-1. Red, JC-1 aggregates; green, JC-1 monomer; blue, nucleus. Scale bar, 10 μm. (F) Reactive oxygen species levels were detected with flow cytometry after 2,7-dichlorfluoresceindiacetate staining. (G) Cell apoptosis was detected with flow cytometry after NDP52 plasmid-transfected HEI-OC1 cells were treated with Neo and Fas. (H) Statistical analysis of flow cytometry. n=6 in each group, each independent experiment was repeated three times. Data are expressed as mean ± SEM. *P<0.05, ***P<0.001. NDP52, nuclear dot protein 52; miR, microRNA; Neo, neomycin; Fas, fasudil.

in the regulation of autophagy by Fas, miR-489 expression was either overexpressed (miR-489 mimic) or knocked down (miR-489 inhibitor) in hair cells, before the cells were treated with Neo and Fas. RT-qPCR was first used to detect the expression of miR-489 in the cells. Neo treatment significantly decreased the expression of miR-489, whereas both Fas and miR-489 mimic significantly increased the level of miR-489 in Neo-treated cells (Fig. 4A). The level of miR-489 expression was significantly decreased in the Neo + Fas + miR-489 inhibitor group compared with the Neo + Fas group. As shown in Fig. 4B and C, the levels of LC3B-II/LC3B-I and Beclin 1 in Neo-treated cells were significantly increased compared with the control group, suggesting enhanced autophagy. Both miR-489 mimic and Fas inhibited the activation of Neo-induced autophagy (Fig. 4B and C). However, compared with the Neo + Fas group, following treatment with the miR-489 inhibitor, Fas could not inhibit Neo-activated autophagy in the Fas + Neo + miR-489 inhibitor group (Fig. 4B and C).

Mitochondrial co-localization experiments demonstrated that mitochondrial autophagy was enhanced in Neo-treated cells, whereas overexpression of miR-489 using the miR-489 mimic and Fas could inhibit the activation of mitochondrial autophagy (Fig. 4D). However, compared with the Neo + Fas group, Fas could not inhibit the activation of mitochondrial autophagy by Neo in the Neo + Fas + miR-489 inhibitor group (Fig. 4D). These results suggested that Fas inhibited mitochondrial autophagy by increasing the level of miR-489 expression. The detection results of mitochondrial membrane potential suggested that both Fas and miR-489 mimic inhibited the Neo-induced reduction in the mitochondrial membrane potential (Fig. 4E). However, the mitochondrial membrane potential in the Neo + Fas group was higher than that in in the Neo + Fas + miR-489 inhibitor group (Fig. 4E).

ROS detection results demonstrated that intracellular ROS levels increased after Neo treatment, whilst ROS levels in cells treated with Fas or miR-489 mimic were markedly lower compared with those induced by Neo alone (Fig. 4F). In the Neo + Fas + miR-489 inhibitor group, Fas failed to inhibit the Neo-induced increase in ROS levels in hair cells (Fig. 4F). The results from flow cytometry showed that the level of apoptosis after Neo treatment was significantly increased, but the level of apoptosis of cells treated with Fas or miR-489

mimic was significantly lower compared with that induced by Neo (Fig. 4G and H). Furthermore, Fas could not inhibit Neo-induced apoptosis in hair cells with miR-489 inhibitor (Fig. 4G and H).

Discussion

Fas is a new isoquinoline sulfonamide derivative, an effective ROCK-II inhibitor and a calcium antagonist (56). Fas is mainly used for clinically treating subarachnoid hemorrhage caused by cerebral vasospasm (57). The present study revealed the inhibitory effects of Fas on Neo-induced inner ear hair cell damage. Further mechanistic studies suggested that Fas reduced the expression of the autophagy-related protein NDP52 at the post-transcriptional level by upregulating the expression of miR-489, thereby inhibiting the activation of Neo-induced autophagy whilst preventing Neo-induced hair cell injury.

The mechanism through which ototoxic drugs cause hair cell damage and apoptosis is complex, though the accumulation of ROS in the cell has been reported to activate multiple signaling pathways associated with apoptosis, such as the ROS/JNK pathway and the caspase-independent apoptosis pathway (58,59), and can serve an important role in inducing hair cell death. For example, mitochondrial calcium uptake is based on ROS generation during aminoglycoside-induced hair cell death (60). Cell survival requires the maintenance of balance between oxidative stress and antioxidant defense systems. When ROS production exceeds the limit of cell repair, cell damage ensues, where ROS accumulation leads to cell death (61,62).

Autophagy is a mechanism for the orderly degradation and renewal of non-essential or damaged cellular components in all eukaryotes (63,64). Autophagosomes engulf organelles or other cytoplasmic components that must be degraded into a bilayer membrane, which then fuse with lysosomes; the contents are degraded through lysosomal hydrolysis (65-67). In certain cases, autophagy can induce autophagic cell death, where the overactivation of autophagy can cause cell death through a variety of degradation pathways, such as macro-autophagy and peroxisome degradation pathways (68). Autophagy attenuates noise-induced hearing loss by reducing oxidative stress (69). Neo can induce hair cell injury, possibly through the increased levels of autophagy in hair cells (43,70). When autophagy occurs, cytoplasmic LC3-I enzymatically cleaves a small polypeptide fragment to become membrane-type LC3-II (48). Therefore, the value of the LC3-II/I ratio may be used to estimate changes in autophagy levels (71).

Results of a previous study demonstrated that Fas regulates autophagy to alleviate cell damage. For example, Fas suppressed TGF-ß-mediated autophagy in urethra fibroblasts of mice to attenuate traumatic urethral stricture (72). Moreover, autophagy inhibition stimulated apoptosis in oesophageal squamous cell carcinoma treated with Fas (73). Thus, the present study aimed to further explore the potential effects of Fas on ototoxicity induced by Neo, and determine whether this was associated with autophagy. HEI-OC1 cells were divided into the control group, Neo group and Neo + Fas group, following which the dose-dependent effects of Fas on Neo-induced apoptosis in cells were assessed via flow cytometry. Further experiments demonstrated that Fas inhibited the increase of mitochondrial autophagy induced by Neo, inhibited the decrease in mitochondrial membrane potential induced by Neo, reduced ROS levels in HEI-OC1 cells and inhibited cell apoptosis.

The mechanism through which Fas regulates autophagy was then investigated. NDP52 is a newly discovered autophagy-related protein that can bind to the LC3 protein on the surface of autophagosomes to promote autophagy (74,75). Gibbings *et al* (75,76) previously found that the expression level of miR-489 was decreased following induction by Neo. The inhibitory effects of Fas on Neo-induced mitochondrial autophagy, mitochondrial membrane potential decline, ROS levels and apoptosis were blocked by the overexpression of NDP52, which was verified in HEI-OC1 cells. It was subsequently explored further how Fas regulated the reduction in NDP52 protein expression. Several bioinformatic analysis software packages were used to predict miRNAs that may target the NDP52 mRNA 3'-UTR. In total, seven miRNAs (miR-9, miR-34a, miR-489, miR-23a, miR-494, miR-93 and miR-214) were screened out by intersecting with previous articles related to deafness and autophagy (31,52-55,77-79). It was predicted and verified that miR-489 could bind to the 3'-UTR of NDP52 mRNA to negatively regulate the expression of NDP52. A series of overexpression and knockdown experiments were also conducted to verify that Fas can inhibit Neo-induced autophagy activation by upregulating the expression of miR-489. This reduced the expression of the autophagy-related protein NDP52 at the post-transcriptional level, thereby inhibiting Neo-induced autophagy activation and preventing Neo-induced hair cell damage.

In conclusion, Fas is a low toxicity drug, which has been widely used in the clinical treatment of postoperative cerebral vasospasm in patients with subarachnoid hemorrhage and acute ischemic stroke (80,81). The findings of the present study suggested that Fas may hold promise as a candidate drug for the prevention and treatment of sensorineural deafness caused by Neo. Furthermore, investigation into the underlying mechanism uncovered that miR-489 may be a potential target for the treatment of drug-induced deafness.

Acknowledgements

Not applicable.

Funding

The present study was funded by the National Natural Science Foundation of China (grant nos. 81970884 and 81771019).

Availability of data and materials

The datasets used and/or analyzed during the current study are available from the corresponding author on reasonable request.

Authors' contributions

WL conceived and designed the current study, performed all experiments and prepared the manuscript. YZ, JC and JX contributed to acquisition, and analysis and interpretation of

data. XG assisted in experimental design, provided general supervision and was responsible for all experimental processes. WL and XG contributed to drafting, critical revision and editing. WL and XG confirmed the authenticity of all the raw data. All authors read and approved the final manuscript.

Ethics approval and consent to participate

Not applicable.

Patient consent for publication

Not applicable.

Competing interests

The authors declare that they have no competing interests.

References

1. Ng M and Horlbeck DM: Sensorineural hearing loss-congenital-genetics. In: Encyclopedia of Otolaryngology, Head and Neck Surgery. Kountakis SE (ed). Springer, Berlin, Heidelberg, 2013.
2. Lin RJ, Krall R, Westerberg BD, Chadha NK and Chau JK: Systematic review and meta-analysis of the risk factors for sudden sensorineural hearing loss in adults. Laryngoscope 122: 624-635, 2012.
3. Arkaravichien W and Schacht J: Drug induced hearing loss: A worldwide problem. Int Med J 4: 243-251, 1997.
4. Cone BK, Wake M, Tobin S, Poulakis Z and Rickards FW: Slight-mild sensorineural hearing loss in children: Audiometric, clinical, and risk factor profiles. Ear Hear 31: 202-212, 2010.
5. Xiong H, Lai L, Ye Y and Zheng Y: Glucose protects cochlear hair cells against oxidative stress and attenuates noise induced hearing loss in mice. Neurosci Bull 37: 657-668, 2021.
6. Ware SL: Human Hearing Loss. PeerJ PrePrints 2: e378v1, 2014.
7. Zhang Y, Li W, He Z, Wang Y, Shao B, Cheng C, Zhang S, Tang M, Qian X, Kong W, *et al*: Pre treatment with fasudil prevents neomycin induced hair cell damage by reducing the accumulation of reactive oxygen speciec. Front Mol Neurosci 12: 264, 2019.
8. Nakagawa T, Yamane H, Takayama M, Sunami K and Nakai Y: Time-dependent response of vestibular hair cells of guinea pigs following high-dose applications of streptomycin. Acta Otolaryngol Suppl 538: 32-35, 1998.
9. Becker B and Cooper MA: Aminoglycoside antibiotics in the 21st century. ACS Chem Biol 8: 105-115, 2013.
10. Brignull HR, Raible DW and Stone JS: Feathers and fins: Non-mammalian models for hair cell regeneration. Brain Res 1277: 12-23, 2009.
11. Chen J, Guan L, Zhu H, Xiong S, Zeng L and Jiang H: Transplantation of mouse-induced pluripotent stem cells into the cochlea for the treatment of sensorineural hearing loss. Acta Otolaryngol 137: 1136-1142, 2017.
12. Kujawa SG and Liberman MC: Synaptopathy in the noise-exposed and aging cochlea: Primary neural degeneration in acquired sensorineural hearing loss. Hear Res 330 (Pt B): 191-199, 2015.
13. Liberman MC: Noise-induced and age-related hearing loss: New perspectives and potential therapies. F1000Res 6: 927, 2017.
14. Géléoc GS and Holt JR: Sound strategies for hearing restoration. Science 344: 1241062, 2014.
15. Chen Y, Huang WG, Zha DJ, Qiu JH, Wang JL, Sha SH and Schacht J: Aspirin attenuates gentamicin ototoxicity: From the laboratory to the clinic. Hear Res 226: 178-182, 2007.
16. Kamogashira T, Fujimoto C and Yamasoba T: Reactive oxygen species, apoptosis, and mitochondrial dysfunction in hearing loss. BioMed Res Int 2015: 617207, 2015.
17. Jiang H, Sha SH and Schacht J: NF-kappaB pathway protects cochlear hair cells from aminoglycoside-induced ototoxicity. J Neurosci Res 79: 644-651, 2005.
18. Momiyama J, Hashimoto T, Matsubara A, Futai K, Namba A and Shinkawa H: Leupeptin, a calpain inhibitor, protects inner ear hair cells from aminoglycoside ototoxicity. Tohoku J Exp Med 209: 89-97, 2006.
19. Yamashita K, Kotani Y, Nakajima Y, Shimazawa M, Yoshimura S, Nakashima S, Iwama T and Hara H: Fasudil, a Rho kinase (ROCK) inhibitor, protects against ischemic neuronal damage in vitro and in vivo by acting directly on neurons. Brain Res 1154: 215-224, 2007.
20. Greathouse KM, Henderson BW, Gentry EG and Herskowitz JH: Fasudil or genetic depletion of ROCK1 or ROCK2 induces anxiety-like behaviors. Behav Brain Res 373: 112083, 2019.
21. Masaoka H, Takasato Y, Nojiri T, Hayakawa T, Akimoto H, Yatsushige H, Toumori H, Miyazaki Y and Honma M: Clinical effect of Fasudil hydrochloride for cerebral vasospasm following subarachnoid hemorrhage. Acta Neurochir Suppl (Wien) 77: 209-211, 2001.
22. Scherer EQ, Arnold W and Wangemann P: Pharmacological reversal of endothelin-1 mediated constriction of the spiral modiolar artery: A potential new treatment for sudden sensorineural hearing loss. BMC Ear Nose Throat Disord 5: 10, 2005.
23. Bonnevier J, Fässler R, Somlyo AP, Somlyo AV and Arner A: Modulation of Ca^{2+} sensitivity by cyclic nucleotides in smooth muscle from protein kinase G-deficient mice. J Biol Chem 279: 5146-5151, 2004.
24. Lesniak W, Pecoraro VL and Schacht J: Ternary complexes of gentamicin with iron and lipid catalyze formation of reactive oxygen species. Chem Res Toxicol 18: 357-364, 2005.
25. Davis RJ: Signal transduction by the JNK group of MAP kinases. Cell 103: 239-252, 2000.
26. Pirvola U, Xing-Qun L, Virkkala J, Saarma M, Murakata C, Camoratto AM, Walton KM and Ylikoski J: Rescue of hearing, auditory hair cells, and neurons by CEP-1347/KT7515, an inhibitor of c-Jun N-terminal kinase activation. J Neurosci 20: 43-50, 2000.
27. Wang J, Van De Water TR, Bonny C, de Ribaupierre F, Puel JL and Zine A: A peptide inhibitor of c-Jun N-terminal kinase protects against both aminoglycoside and acoustic trauma-induced auditory hair cell death and hearing loss. J Neurosci 23: 8596-8607, 2003.
28. Eshraghi AA, Wang J, Adil E, He J, Zine A, Bublik M, Bonny C, Puel JL, Balkany TJ and Van De Water TR: Blocking c-Jun-N-terminal kinase signaling can prevent hearing loss induced by both electrode insertion trauma and neomycin ototoxicity. Hear Res 226: 168-177, 2007.
29. Yuan B, Yu WY, Dai LS, Gao Y, Ding Y, Yu XF, Chen J and Zhang JB: Expression of microRNA 26b and identification of its target gene EphA2 in pituitary tissues in Yanbian cattle. Mol Med Rep 12: 5753-5761, 2015.
30. Beisel K, Hansen L, Soukup G and Fritzsch B: Regenerating cochlear hair cells: Quo vadis stem cell. Cell Tissue Res 333: 373-379, 2008.
31. Geng W and Liu L: miR-494 alleviates lipopolysaccharide (LPS)-induced autophagy and apoptosis in PC-12 cells by targeting IL-13. Adv Clin Exp Med 28: 85-94, 2019.
32. Kuhn S, Johnson SL, Furness DN, Chen J, Ingham N, Hilton JM, Steffes G, Lewis MA, Zampini V, Hackney CM, *et al*: miR-96 regulates the progression of differentiation in mammalian cochlear inner and outer hair cells. Proc Natl Acad Sci USA 108: 2355-2360, 2011.
33. Ghasemi-Dehkordi P, Allahbakhshian-Farsani M, Abdian N, Mirzaeian A, Saffari-Chaleshtori J, Heybati F, Mardani G, Karimi-Taghanaki A, Doosti A, Jami MS, *et al*: Comparison between the cultures of human induced pluripotent stem cells (hiPSCs) on feeder-and serum-free system (Matrigel matrix), MEF and HDF feeder cell lines. J Cell Commun Signal 9: 233-246, 2015.
34. Zhang B, Ji S, Ma F, Ma Q, Lu X and Chen X: miR-489 acts as a tumor suppressor in human gastric cancer by targeting PROX1. Am J Cancer Res 6: 2021-2030, 2016.
35. Patel Y, Shah N, Lee JS, Markoutsa E, Jie C, Liu S, Botbyl R, Reisman D, Xu P and Chen H: A novel double-negative feedback loop between miR-489 and the HER2-SHP2-MAPK signaling axis regulates breast cancer cell proliferation and tumor growth. Oncotarget 7: 18295-18308, 2016.
36. Li J, Qu W, Jiang Y, Sun Y, Cheng Y, Zou T and Du S: miR-489 suppresses proliferation and invasion of human bladder cancer cells. Oncol Res 24: 391-398, 2016.
37. Soni M, Patel Y, Markoutsa E, Jie C, Liu S, Xu P and Chen H: Autophagy, cell viability, and chemoresistance are regulated by miR 489 in breast cancer. Mol Cancer Res 16: 1348-1360, 2018.
38. Liao CC, Ho MY, Liang SM and Liang CM: Autophagic degradation of SQSTM1 inhibits ovarian cancer motility by decreasing DICER1 and AGO2 to induce MIRLET7A-3P. Autophagy 14: 2065-2082, 2018.

39. Livak KJ and Schmittgen TD: Analysis of relative gene expression data using real-time quantitative PCR and the 2(-ΔΔC(T)) method. Methods 25: 402-408, 2001.
40. Fischel-Ghodsian N: Genetic factors in aminoglycoside toxicity. Pharmacogenomics 6: 27-36, 2005.
41. Zheng Z, Tang D, Zhao L, Li W, Han J, Hu B, Nie G and He Y: Liproxstatin 1 protects hair cell like HEI OC1 cells and cochlear hair cells against neomycin ototoxicity. Oxid Med Cell Longev 2020: 1782659, 2020.
42. Mortimore GE and Pösö AR: Intracellular protein catabolism and its control during nutrient deprivation and supply. Annu Rev Nutr 7: 539-564, 1987.
43. He Z, Guo L, Shu Y, Fang Q, Zhou H, Liu Y, Liu D, Lu L, Zhang X, Ding X, *et al*: Autophagy protects auditory hair cells against neomycin-induced damage. Autophagy 13: 1884-1904, 2017.
44. Djavaheri-Mergny M, Amelotti M, Mathieu J, Besançon F, Bauvy C, Souquère S, Pierron G and Codogno P: NF-kappaB activation represses tumor necrosis factor-alpha-induced autophagy. J Biol Chem 281: 30373-30382, 2006.
45. Lee Y, Ahn C, Han J, Choi H, Kim J, Yim J, Lee J, Provost P, Rådmark O, Kim S, *et al*: The nuclear RNase III Drosha initiates microRNA processing. Nature 425: 415-419, 2003.
46. Chendrimada TP, Gregory RI, Kumaraswamy E, Norman J, Cooch N, Nishikura K and Shiekhattar R: TRBP recruits the Dicer complex to Ago2 for microRNA processing and gene silencing. Nature 436: 740-744, 2005.
47. Ameres SL and Zamore PD: Diversifying microRNA sequence and function. Nat Rev Mol Cell Biol 14: 475-488, 2013.
48. Forman JJ and Coller HA: The code within the code: microRNAs target coding regions. Cell Cycle 9: 1533-1541, 2010.
49. Lytle JR, Yario TA and Steitz JA: Target mRNAs are repressed as efficiently by microRNA-binding sites in the 5' UTR as in the 3' UTR. Proc Natl Acad Sci USA 104: 9667-9672, 2007.
50. Meister G, Landthaler M, Patkaniowska A, Dorsett Y, Teng G and Tuschl T: Human Argonaute2 mediates RNA cleavage targeted by miRNAs and siRNAs. Mol Cell 15: 185-197, 2004.
51. Mizushima N: Autophagy: Process and function. Genes Dev 21: 2861-2873, 2007.
52. Li W, Yang Y, Ba Z, Li S, Chen H, Hou X, Ma L, He P, Jiang L, Li L, *et al*: MicroRNA-93 regulates hypoxia-induced autophagy by targeting ULK1. Oxid Med Cell Longev 2017: 2709053, 2017.
53. Liu L, Ren W and Chen K: miR-34a promotes apoptosis and inhibits autophagy by targeting HMGB1 in acute myeloid leukemia cells. Cell Physiol Biochem 41: 1981-1992, 2017.
54. Si X, Cao D, Chen J, Nie Y, Jiang Z, Chen MY, Wu JF and Guan XD: miR 23a downregulation modulates the inflammatory response by targeting ATG12 mediated autophagy. Mol Med Rep 18: 1524-1530, 2018.
55. Zhou DM, Sun LL, Zhu J, Chen B, Li XQ and Li WD: miR-9 promotes angiogenesis of endothelial progenitor cell to facilitate thrombi recanalization via targeting TRPM7 through PI3K/Akt/autophagy pathway. J Cell Mol Med 24: 4624-4632, 2020.
56. Dulon D, Hiel H, Aurousseau C, Erre JP and Aran JM: Pharmacokinetics of gentamicin in the sensory hair cells of the organ of Corti: Rapid uptake and long term persistence. C R Acad Sci III 316: 682-687, 1993.
57. Lemasters JJ: Selective mitochondrial autophagy, or mitophagy, as a targeted defense against oxidative stress, mitochondrial dysfunction, and aging. Rejuvenation Res 8: 3-5, 2005.
58. Holze C, Michaudel C, Mackowiak C, Haas DA, Benda C, Hubel P, Pennemann FL, Schnepf D, Wettmarshausen J, Braun M, *et al*: Oxeiptosis, a ROS-induced caspase-independent apoptosis-like cell-death pathway. Nat Immunol 19: 130-140, 2018.
59. Wang Z, Yu K, Hu Y, Su F, Gao Z, Hu T, Yang Y, Cao X and Qian F: Schisantherin A induces cell apoptosis through ROS/JNK signaling pathway in human gastric cancer cells. Biochem Pharmacol 173: 113673, 2020.
60. Esterberg R, Linbo T, Pickett SB, Wu P, Ou HC, Rubel EW and Raible DW: Mitochondrial calcium uptake underlies ROS generation during aminoglycoside-induced hair cell death. J Clin Invest 126: 3556-3566, 2016.
61. Platini F, Pérez-Tomás R, Ambrosio S and Tessitore L: Understanding autophagy in cell death control. Curr Pharm Des 16: 101-113, 2010.
62. Su Z, Yang Z, Xu Y, Chen Y and Yu Q: Apoptosis, autophagy, necroptosis, and cancer metastasis. Mol Cancer 14: 48, 2015.
63. Sheth S, Mukherjea D, Rybak LP and Ramkumar V: Mechanisms of cisplatin induced ototoxicity and otoprotection. Front Cell Neurosci 11: 338, 2017.
64. Tabuchi K, Nishimura B, Nakamagoe M, Hayashi K, Nakayama M and Hara A: Ototoxicity: Mechanisms of cochlear impairment and its prevention. Curr Med Chem 18: 4866-4871, 2011.
65. Niwa K, Matsunobu T, Kurioka T, Kamide D, Tamura A, Tadokoro S, Satoh Y and Shiotani A: The beneficial effect of Hangesha-shin-to (TJ-014) in gentamicin-induced hair cell loss in the rat cochlea. Auris Nasus Larynx 43: 507-513, 2016.
66. Choung YH, Taura A, Pak K, Choi SJ, Masuda M and Ryan AF: Generation of highly-reactive oxygen species is closely related to hair cell damage in rat organ of Corti treated with gentamicin. Neuroscience 161: 214-226, 2009.
67. Vernon PJ and Tang D: Eat-me: Autophagy, phagocytosis, and reactive oxygen species signaling. Antioxid Redox Signal 18: 677-691, 2013.
68. Wang X, Wang P, Zhang Z, Farré JC, Li X, Wang R, Xia Z, Subramani S and Ma C: The autophagic degradation of cytosolic pools of peroxisomal proteins by a new selective pathway. Autophagy 16: 154-166, 2020.
69. Yuan H, Wang X, Hill K, Chen J, Lemasters J, Yang SM and Sha SH: Autophagy attenuates noise-induced hearing loss by reducing oxidative stress. Antioxid Redox Signal 22: 1308-1324, 2015.
70. Oh KH, Rah YC, Hwang KH, Lee SH, Kwon SY, Cha JH and Choi J: Melatonin mitigates neomycin-induced hair cell injury in zebrafish. Drug Chem Toxicol 40: 390-396, 2017.
71. Lee Y, Jeon K, Lee JT, Kim S and Kim VN: MicroRNA maturation: Stepwise processing and subcellular localization. EMBO J 21: 4663-4670, 2002.
72. Feng H, Huang X, Fu W, Dong X, Yang F, Li L and Chu L: A Rho kinase inhibitor (Fasudil) suppresses TGF-β mediated autophagy in urethra fibroblasts to attenuate traumatic urethral stricture (TUS) through re-activating Akt/mTOR pathway: An in vitro study. Life Sci 267: 118960, 2021.
73. Xie FJ, Zheng QQ, Qin J, Zhang LL, Han N and Mao WM: Autophagy inhibition stimulates apoptosis in oesophageal squamous cell carcinoma treated with fasudil. J Cancer 9: 1050-1056, 2018.
74. Falcon B, Noad J, McMahon H, Randow F and Goedert M: Galectin-8-mediated selective autophagy protects against seeded tau aggregation. J Biol Chem 293: 2438-2451, 2018.
75. Gibbings D, Mostowy S and Voinnet O: Autophagy selectively regulates miRNA homeostasis. Autophagy 9: 781-783, 2013.
76. Gibbings D, Mostowy S, Jay F, Schwab Y, Cossart P and Voinnet O: Selective autophagy degrades DICER and AGO2 and regulates miRNA activity. Nat Cell Biol 14: 1314-1321, 2012. Erratum in: Nat Cell Biol 17: 1088, 2015.
77. Hu JL, He GY, Lan XL, Zeng ZC, Guan J, Ding Y, Qian XL, Liao WT, Ding YQ and Liang L: Inhibition of ATG12-mediated autophagy by miR-214 enhances radiosensitivity in colorectal cancer. Oncogenesis 7: 16, 2018.
78. Sivakumaran TA, Resendes BL, Robertson NG, Giersch AB and Morton CC: Characterization of an abundant COL9A1 transcript in the cochlea with a novel 3' UTR: Expression studies and detection of miRNA target sequence. J Assoc Res Otolaryngol 7: 160-172, 2006.
79. Xiong H, Chen S, Lai L, Yang H, Xu Y, Pang J, Su Z, Lin H and Zheng Y: Modulation of miR-34a/SIRT1 signaling protects cochlear hair cells against oxidative stress and delays age-related hearing loss through coordinated regulation of mitophagy and mitochondrial biogenesis. Neurobiol Aging 79: 30-42, 2019.
80. Masumoto A, Mohri M, Shimokawa H, Urakami L, Usui M and Takeshita A: Suppression of coronary artery spasm by the Rho-kinase inhibitor fasudil in patients with vasospastic angina. Circulation 105: 1545-1547, 2002.
81. Shibuya M, Hirai S, Seto M, Satoh S and Ohtomo E; Fasudil Ischemic Stroke Study Group: Effects of fasudil in acute ischemic stroke: Results of a prospective placebo-controlled double-blind trial. J Neurol Sci 238: 31-39, 2005.